Dynamics of Interaction of Magnesium Atoms on Methoxy-Terminated Self-Assembled Monolayers: An Example of a Reactive Metal with a Low Sticking Probability

Amy V. Walker,*,† Timothy B. Tighe,‡ Orlando Cabarcos, Brendan C. Haynie,§ David L. Allara,* and Nicholas Winograd*

Department of Chemistry, The Pennsylvania State University, 184 Materials Research Institute, University Park, Pennsylvania 16802

Received: July 11, 2006; In Final Form: October 1, 2006

The collision of low-flux vapor-generated Mg atoms with a methoxy-terminated self-assembled monolayer (SAM) at room temperature results primarily in nonreactive scattering from the surface. Those atoms that adsorb undergo reaction via O−C bond insertion to form Mg−O−R products, with an estimated activation energy of 38 ± 9 kJ mol^{-1}. These products, in turn, provide nucleation sites for the subsequent formation of Mg clusters. As growth continues, a nonuniform Mg overlayer eventually forms. These behaviors contrast with that of vapor-deposited Al (which shows a high sticking probability and low chemical reactivity under the same experimental conditions). This behavior is consistent with quantum chemical predictions of differences in the ability of the $-OCH_3$ group to stabilize these metal atoms. Overall, these results highlight the importance of dynamic processes in controlling the interfacial chemistry and metal overlayer morphology in vapor-deposited films on organic surfaces.

1. Introduction

Understanding of the interaction of metals with organic materials is becoming increasingly important for a wide variety of technological applications including molecular/organic electronics. Self-assembled monolayers (SAMs) are a broadly applicable, chemically and structurally variable platform, with a wide variety of terminal group functionalities available. Recent work has shown that SAMs can be used to significant advantage in fundamental studies of the formation and characteristics metal−organic interfaces.[1−7] In addition, metal−SAM constructs have potential as electronic devices.[8−10]

To rationally design and predict the behavior of metal−organic structures, it is necessary to have a fundamental understanding of the dynamics of the metal atom interaction with these surfaces. In the earliest stages of deposition, the organic layer must accommodate some fraction of the kinetic energy of the impinging metal atom. Recent studies by Morris and co-workers[11−16] have demonstrated that the energy accommodation on SAM surfaces is dependent on the chemical nature and energy of the impinging atom/molecule and the identity of the SAM terminal group. For example, at low incident kinetic energy (6 kJ mol^{-1}, 0.06 eV), HCl molecules impinging on an −OH-terminated SAM are temporarily trapped on the surface via the formation of HO−HCl hydrogen bonds.[15] Subsequent surface processes are determined by this energy accommodation.[17,18] After surface collision, the gaseous species might lack enough momentum to escape the gas−surface potential well and can become trapped on the surface. These adsorbed atoms can diffuse across the surface and eventually react. Other adsorbates might react with the surface close to the point of impact or scatter directly from the surface. A useful parameter for investigating the dynamics of the gas−surface interaction is the sticking probability (or condensation coefficient). The sticking probability, *S*, is defined as

$$S = \frac{N_{\text{ads}}}{N_{\text{total}}}$$

where N_{ads} and N_{total} are the number of adsorbed metal atoms and the number of impinging metal atoms, respectively. Sticking coefficients have been extensively studied on metal surfaces[19] using, for example, the King and Wells method.[20] However, far less is known about the sticking probability of metals on organic surfaces. There is some evidence for significant variations in the sticking coefficients. For example, Faupel and co-workers recently examined the interaction of vapor-deposited Cu, Ag, and Au with a variety of polymers and determined that the sticking probability varied from 0.95 [on pyromellitic dianhydride−oxydianiline (PMDA−ODA) polyimide] to 0.002 (on Teflon).[21−24]

Although magnesium metallization is not generally thought to be of practical value, Mg is being considered as an electrode in the fabrication of polymer light-emitting diodes (PLEDs) because it has a low work function. Thus, a few studies have been conducted on the interaction of magnesium with polymers such as polyalanine (PANI),[25,26] polyethyleneterephthlate (PET),[27,28] polypyrrole (PPY),[29] poly(*p*-phenylene vinylene) (PPV),[30,31] Nafion,[32] and polyprolylene.[33−36] In all cases, the deposited magnesium was observed to react preferentially with O to form Mg−O bonds and not to penetrate into the polymer film. However, we also note that it was reported that a significant amount of magnesium was deposited before magnesium could be observed at the polymer/vacuum (air) interface, indicating

* Corresponding authors. E-mail: dla3@psu.edu (D.L.A.), walker@wuchem.wustl.edu (A.V.W.), nxw@psu.edu (N.W). Fax: 814-863-0618 (D.L.A.), 314-935-4481 (A.V.W.), 814-863-0618 (N.W).

† Present address: Department of Chemistry, Washington University, Campus Box 1134, St. Louis, MO 63130.

‡ Present address: Motorola Labs, 2100 E. Elliot Road, Tempe, AZ 85284.

§ Present address: School of Arts and Sciences, Kentucky Christian University, 100 Academic Parkway, Grayson, KY 41143.

10.1021/jp064372r CCC: $37.00 © 2007 American Chemical Society
Published on Web 11/18/2006

that Mg has a low sticking probability on these films.[29,31] Nowak, Collaud, and Schlapbach observed that the sticking coefficient of Mg on polypropylene varied between 0 and a maximum value of 0.3 ± 0.2 depending on the polymer surface preparation.[33−36]

In a previous study, we observed that the reactivity of Al with a $-OCH_3$ alkanethiolate is intermediate between those observed for a $-CH_3$-terminated SAM and for the more reactive $-CO_2CH_3$, $-$COOH, and $-$OH-terminated SAMs.[5−7] Al forms a weak complex with the $-OCH_3$-terminated SAM, Al···OCH_3, and also penetrates to the Au/S interface. Thus, this type of SAM is an ideal monolayer for determining how the nature of the metal−organic interaction can be changed, and ultimately controlled, by the reactivity of the deposited metal atoms such as Mg.

In the present work, infrared spectroscopy (IRS), time-of-flight secondary ion mass spectrometry (TOF SIMS), X-ray photoelectron spectroscopy (XPS), and density functional theory (DFT) calculations are employed to investigate the interfacial chemistry of vapor-deposited magnesium with a methoxy-terminated hexadecanethiol SAM on Au{111}. Under our experimental conditions, i.e., a room-temperature sample and a Mg flux of $\sim$0.15 atoms nm^{-2} s^{-1}, Mg has a very low initial sticking probability, $\sim 5 \times 10^{-3}$. The adsorption process consists of reaction with a $-OCH_3$ terminal group to produce a Mg−O−R complex, suggesting that Mg adsorption is an activated process. From our data, we estimate that the associated activation barrier is 38 ± 9 kJ mol^{-1}.

This behavior is very different from that observed for aluminum with $-OCH_3$-terminated SAMs. Al efficiently adsorbs on the SAM surface and subsequently partitions between the formation of a weak Al···OCH_3 complex and penetration to the Au/S interface.[5−7] Aluminum and magnesium have very similar bulk reactivities; both metals displace hydrogen from steam and tarnish in air. Using quantum chemical calculations, we show that the different behaviors can be attributed to differing types of interaction with the $-OCH_3$ group. Magnesium is unable to form a stable Mg···OCH_3 complex; rather, the preferred reaction pathway is to insert into the C−O bond. There is a significant activation barrier for this process, and consequently, most of the impinging Mg atoms scatter from the surface. In the case of Al, the reaction barrier for insertion into the C−O bond is much larger, and so, the reaction product is always Al···OCH_3.[5−7] This stabilizes the impinging Al atoms at the SAM/vacuum interface, leading to efficient adsorption. These data demonstrate the subtle effect of competing surface processes in determining the overall characteristics of metal deposition.

2. Experimental Section

2.1. Materials and General Procedures. The preparation and characterization of the type of SAM used in this study has been described in detail previously.[5,37−42] The metals for all depositions were obtained from Goodfellow, R. D. Mathis, and Alfa Aesar and were of $\geq$99.99% purity.

2.2. SAM Preparation. Cr ($\sim$5 nm) and Au ($\sim$200 nm) were sequentially thermally deposited onto clean Si(001) native-oxide-covered wafers. Self-assembly of well-organized monolayers was achieved by immersing the Au substrates into millimolar solutions of the relevant methoxyhexadecanethiol molecule in absolute ethanol for $\sim$2 days at ambient temperature. The monolayer films were characterized with single-wavelength ellipsometry, infrared spectroscopy, and contact angle measurements to ensure that they were densely packed with clean surfaces. In addition, all SAMs were characterized by initial TOF SIMS, XPS, and IRS measurements prior to metal deposition.

2.3. Time-of-Flight Secondary Ion Mass Spectrometry. The TOF SIMS analyses were performed on a custom-designed instrument that has been described in detail previously.[43] Briefly, the instrument consists of a loadlock, a preparation chamber, a metal deposition chamber, and the primary analysis chamber, each separated by a gate valve. Primary Ga^+ ions were accelerated to 15 keV and contained in a 100-nm-diameter probe beam that was rastered over a 106×106 μm^2 area during data acquisition. All spectra were acquired using a total ion dose of less than 10^{11} ions·cm^{-2}. Relative peak intensities are reproducible to within $\pm$10% from sample to sample and $\pm$8% from scan to scan.

Magnesium was deposited onto the sample at room temperature from a W-wire basket source at a rate of $\sim$0.15 atoms·nm^{-2}·s^{-1} with the pressure maintained below 5×10^{-8} Torr. After deposition, the preparation chamber pressure was allowed to recover to the base value of 1.5×10^{-9} Torr before sample transfer to the analysis chamber. The deposited mass/area was monitored using a quartz crystal microbalance (QCM; TM-400 controller, Maxtek Inc.) with a maximum error of within $\pm$8%.

2.4. Infrared Spectroscopy. Analyses were performed on a Fourier transform instrument (Mattson Research Series 1000) fitted with custom in-house optics configured external to the instrument and designed for grazing-incidence reflection of samples under vacuum.[3−6] A liquid-nitrogen-cooled MCT detector was used with an effective low-frequency cutoff of $\sim$750 cm^{-1}. The infrared beam was allowed to access the vacuum system and reflect from the sample through a pair of differentially pumped KBr windows. After analysis of the bare monolayer, a shield was moved to unblock the path between the sample and the metal source. Magnesium was evaporated in the same way and at the same average rate as for the TOF SIMS experiments. The chamber pressure remained below 1×10^{-7} Torr during deposition. Relative peak intensities were reproducible to within $\pm$2% from sample to sample and $\pm$2% from scan to scan.

2.5. X-ray Photoelectron Spectroscopy. The XPS analyses were performed on a spectrometer (Scienta ESCA 300) equipped with a monochromatic Al Kα source, as described in detail elsewhere.[44,45] A pass energy of 75 eV and an energy step of 0.05 eV were used for the analysis. The resulting full width at half-maximum (fwhm) for Au $4f_{7/2}$ is 0.52 eV. A binding energy of 84.00 eV for Au $4f_{7/2}$ was used as a reference for all spectra.

Following analysis of the uncoated monolayer, the sample was transferred under vacuum to the deposition chamber, which was isolated from the analysis chamber by a gate valve. The pressure in the preparation chamber remained below 5×10^{-8} Torr during deposition. Magnesium was deposited at a highly controlled, constant rate, typically $\sim$0.15 atoms·nm^{-2}·s^{-1} as monitored by a QCM, by evaporation from a graphite crucible. After deposition, the metal/SAM specimen was transferred directly under vacuum to the analysis chamber, where the pressure was maintained below 1×10^{-8} Torr.

2.6. Quartz Crystal Microbalance (QCM) Measurements. *2.6.1. Definition of Deposited Metal Coverage.* The metal deposition onto the samples was monitored directly as the mass per unit area by a QCM. For ease in data analysis and interpretation, the deposited amounts were converted to a dose of metal atoms per SAM molecule, designated θ_{Mg}. The SAM molecular density is 4.6 molecules nm^{-2} in a well-formed

alkanethiolate/Au{111} SAM.[40] Thus, for $\theta_{Mg} = 1.0$, there would be one magnesium atom dosed on average per SAM molecule.

2.6.2. Sticking Probability Measurements. To determine the sticking probability of vapor-deposited Mg on the $-OCH_3$-terminated SAM, a dual-QCM experiment was performed. Two QCMs, one coated with a $-OCH_3$-terminated SAM, were exposed to a Mg vapor deposition source, and an amount of Mg was deposited on each QCM. By comparing the change in frequency on each QCM (which is proportional to the mass of Mg deposited), the sticking probability of Mg was calculated

$$\text{sticking probability} = \frac{\text{change in frequency of the } -OCH_3 \text{ SAM-coated QCM}}{\text{change in frequency of the reference QCM}}$$

Using the Sauerbray equation,[46] a coverage of 1 ML of Mg (4.6×10^{14} molecules·cm^{-2} [40]) is equivalent to a frequency change of ~1.5 Hz on a QCM oscillating at 6 MHz, so it is important to obtain very accurate frequency measurements. For this reason, a custom-built phase-locked-loop QCM apparatus was employed.[47] This allowed us to obtain measurements accurate to ±0.05 Hz.

All experiments were performed in a vacuum chamber with a base pressure of $\sim 2 \times 10^{-8}$ Torr. The Mg was deposited from a W-wire basket at the same rate as for the TOF SIMS, IRS, and XPS experiments. The reference QCM crystal was a standard gold 6-MHz crystal (Cold Springs R&D Inc.) and was maintained at 10 °C using recirculated laboratory-chilled water. The SAM-coated QCM was maintained at 25.0 ± 0.1 °C using a temperature bath (RTE-110 Temperature Bath/Circulator, Neslab Inc.). These temperatures were maintained throughout the experiment to mimic the deposition conditions used in the IRS and TOF SIMS measurements. The SAM-coated QCM was prepared in the following way: A single-sided polished 6-MHz QCM crystal was stripped of its gold electrodes, and the electrodes were redeposited to ensure the quality of the gold film. A methoxy-terminated SAM was then adsorbed on the Au-coated crystal using the procedure described in section 2.1. To check the quality of the films produced, "companion" samples were made using the same procedure and then characterized by IRS and single-wavelength ellipsometry.

The sticking probability measurements were performed using the following procedure: The two QCMs were placed equidistant from a Mg vapor-deposition source. A shutter was placed over the $-OCH_3$-terminated SAM-coated QCM, and ~500 Å of Mg was vapor-deposited on the reference QCM. This procedure ensured that the sticking probability on the reference was unity and also allowed for a steady-state deposition rate to be obtained. The shutter was then opened, and both QCMs were exposed to the Mg vapor. The experiment was concluded when the rates of frequency change measured by each QCM were the same.

2.7. Quantum Chemical Calculations. Density functional theory (DFT) calculations were performed to provide estimates of the interaction of magnesium and aluminum with the terminal group of the $-OCH_3$ SAM. Calculations were carried out using the Gaussian 98 (revision A.9) program.[48] The calculations were carried out on the following systems: $M + CH_3O-(CH_2)_5-SH$ and $M-O-(CH_2)_5-SH$, where M = Mg, Al. The SAM was truncated by 11 methylene units and modeled as $CH_3O-(CH_2)_5-SH$ to reduce the computational cost. The missing subunits are not expected to significantly affect the calculated bond energies, as intramolecular induction effects typically range over 2−3 bonds. Geometry optimizations and frequency calculations were performed at the B3PW91/6-31G* level of theory. All energies are reported as enthalpies of the final structures relative to the isolated reactants and contain zero-point-energy and thermal-energy corrections for standard temperature and pressure.

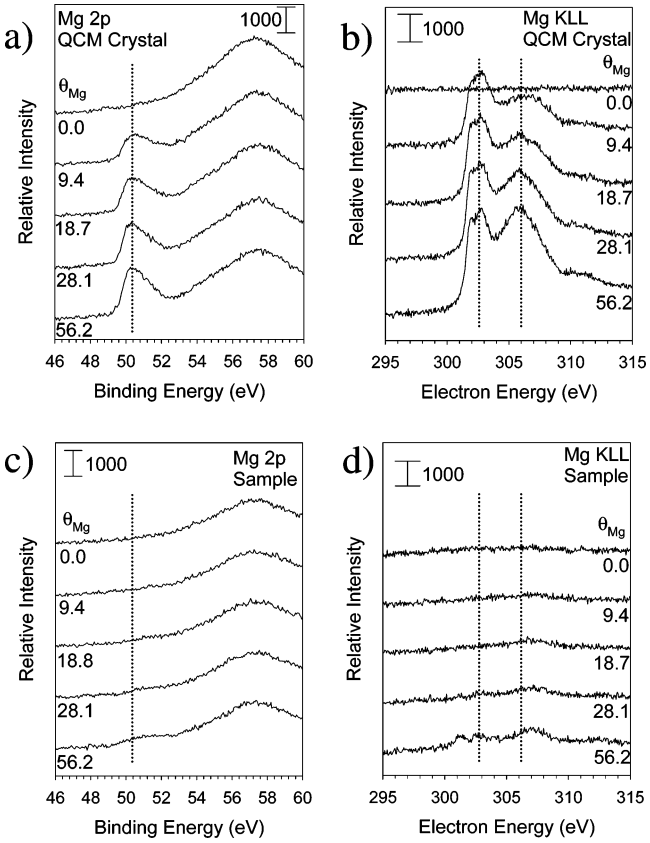

Figure 1. High-resolution spectra of Mg 2p XPS and Mg KLL Auger peaks on the QCM crystal (bare gold) and the methoxy-terminated SAM upon Mg deposition. The dotted lines are intended to guide the eye and mark the positions of the Mg 2p XPS and Mg KLL Auger lines.

3. Results

3.1. Sticking Coefficient Measurements. The results from the preliminary IRS and TOF SIMS experiments suggested that the sticking probability of Mg on $-OCH_3$-terminated SAMs was very low. We tested this hypothesis by carrying out the following experiment using XPS (Figure 1): We placed a bare gold QCM crystal and a methoxy-terminated SAM on the same sample holder and simultaneously deposited ~60 Å Mg ($\theta_{Mg} \approx 56$) on each sample. We then measured the intensity of the Mg 2p XPS and KLL Auger peaks. Because the two samples were side-by-side on the same holder, equidistant from the deposition source, the two samples received the same dose of Mg. On the QCM crystal, we observed both a Mg 2p XPS peak (50 eV) and Mg KLL Auger peaks (302.4 and 306 eV; kinetic energy = 1184.2 and 1180.6 eV). In contrast, on the $-OCH_3$-terminated alkanethiolate, a trace intensity in the Mg 2p XPS peak and a very small Mg KLL Auger peak were observed. These observations confirmed that, under our experimental conditions, vapor-deposited Mg has a low sticking probability on $-OCH_3$-terminated SAMs.

To try to measure the sticking probability, we performed dual-QCM measurements (see section 2.6.2). The initial sticking probability measured at a surface Mg coverage of 0.4 ML was $\sim 5 \times 10^{-3}$.[49] As the Mg vapor deposition continued, the sticking probability rapidly increased as a Mg overlayer nucleated on

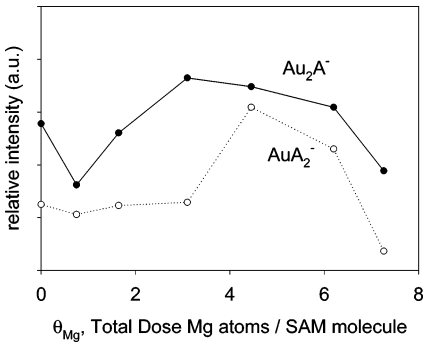

Figure 2. Peak intensities of the molecular adsorbate ions Au_2A^- and AuA_2^- ions, where $A = S(CH_2)_{16}OCH_3$, plotted versus θ_{Mg}.

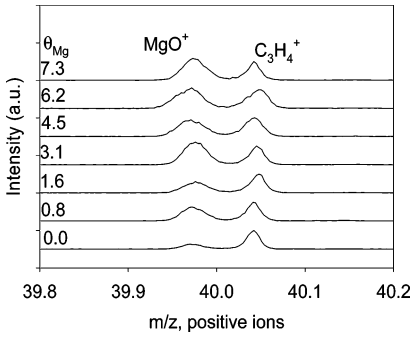

Figure 3. High-resolution SIMS spectral overlays of MgO^+ fragments, nominal mass 40 amu, with increasing Mg dose. The intensity is normalized to the initial peak intensity of $C_3H_4^+$.

the surface. At a surface coverage of 5 ML (total Mg dose, θ_{Mg} = 100 ML), the sticking coefficient was 0.05. By a surface coverage of 10 ML (total Mg dose, θ_{Mg} = 200 ML), the sticking probability had risen to 0.15.

3.2. TOF SIMS. TOF SIMS is a very surface-sensitive technique and so was used to probe the low-Mg-dose regime (0−8 ML Mg dose), where the sticking probability is $\sim 5 \times 10^{-3}$, to investigate the interaction of Mg with a bare $-OCH_3$ SAM surface. The intensity of the molecular ions, Au_2A^- and AuA_2^-, where $A = -S(CH_2)_{16}OCH_3$, give an indication of whether the deposited Mg reacts with the methoxy-terminated SAM monolayer.[3−5,7] The intensity of these ions fluctuates over a very narrow range over the whole deposition range, as shown in Figure 2. This observation supports the conclusion that Mg has a low sticking probability on the $-OCH_3$-terminated SAM surface. Consistent with this interpretation, the hydrocarbon fragment-ion intensities remain approximately constant during the early stages of deposition (data not shown).

In the positive mass spectrum, we observe the formation of MgO^+ ions (m/z = 39.98) with increasing Mg dose (Figure 3). The spectra are normalized to the initial peak intensities of $C_3H_4^+$ in order to make obvious the changing intensities of the peaks with respect to the hydrocarbon and substrate fragments as the deposition progresses. We also note the slight intensity at 39.98 Da for the bare SAM monolayer (0.0 Mg atoms/SAM molecule). This is a contaminant peak and is identified as KH^+ arising from a small amount of potassium that is always present in our samples. *Neither* $MgOCH_3^+$ *nor* $MgSH_2^+$ are observed (data not shown). Based on our previous work with −COOH-terminated[4] and $-CO_2CH_3$-terminated[3] SAMs, the appearance of MO^+ indicates that the deposited Mg has undergone a redox reaction with the methoxy functionality to form M−O bonds. The absence of a $MgSH_2^+$ peak suggests that vapor-deposited Mg does not penetrate to the Au/S interface.[3−5,7] Thus, the data suggest that the deposited Mg atoms undergo a chemical reaction

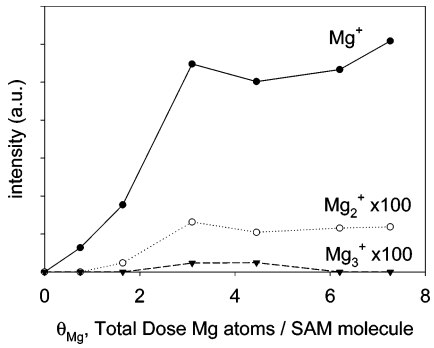

Figure 4. Peak intensity of Mg_n^+, n = 1−3, areas plotted versus θ_{Mg} for the $-OCH_3$ SAM.

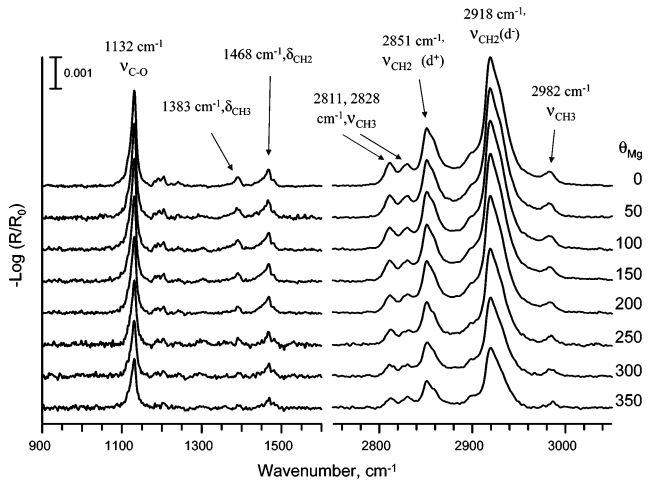

Figure 5. Low- and high-frequency regions of the IR spectra of the $-OCH_3$-terminated SAM for increasing values of θ_{Mg}.

with the terminal group to form a R−O−Mg complex [where R = $-(CH_2)-$ backbone of the alkanethiolate].

Further evidence of the interaction of Mg with the $-OCH_3$ alkanethiolate can be found by examining the intensities of Mg_n^+ (n = 1−3) clusters as a function of Mg dose (Figure 4). Upon deposition of the first increment of Mg, only the Mg^+ signal increases; appreciable levels of Mg_2^+ and Mg_3^+ appear at θ_{Mg} > 1.6 ML. Judging from our previous studies,[3,4] these observations can be interpreted in the following way: At the lowest Mg coverages, the Mg overlayer consists primarily of isolated Mg atoms bound to the $-OCH_3$ groups. The appearance of Mg_2^+ and Mg_3^+ indicates that the deposition of additional Mg initiates the formation of scattered islands. Because the amount of adsorbed Mg atoms at these Mg doses is very small, the probability of an impinging Mg atom adsorbing on an existing Mg site is low. This suggests that the nucleation of Mg islands might arise via the diffusion of adsorbed Mg atoms. It is likely that the fraction of physisorbed (i.e., unreacted) Mg is very low because there is no evidence of a weak Mg/$-OCH_3$ terminal group interaction.

3.3. IRS. IR spectra of the methoxy-terminated SAM, before and after Mg deposition, are shown in Figure 5. The peak assignments of the bare monolayer have been reported previously[5,39,50,51] and are summarized here. The peaks at 1132, 1390, and 1465 cm^{-1} are assigned as the C−O−C antisymmetric stretch (ν_{C-O}), the $-CH_3$ symmetric deformation (δ_{CH_3}), and the $-CH_2-$ scissor deformation (δ_{CH_2}), respectively. In the high-frequency regime, the $-CH_2-$ d^+ and d^- stretches (ν_{CH_2}) are assigned at 2851 and 2918 cm^{-1}. The peaks at 2811, 2828, and 2981 cm^{-1} are attributed to various stretching modes of the terminal CH_3 group. The data indicate that the bare monolayer

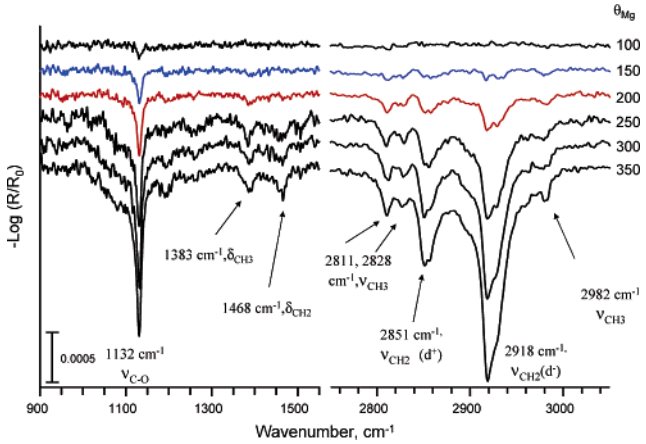

Figure 6. IR difference spectra of the $-OCH_3$-terminated SAM upon Mg deposition for $\theta_{Mg} > 100$.

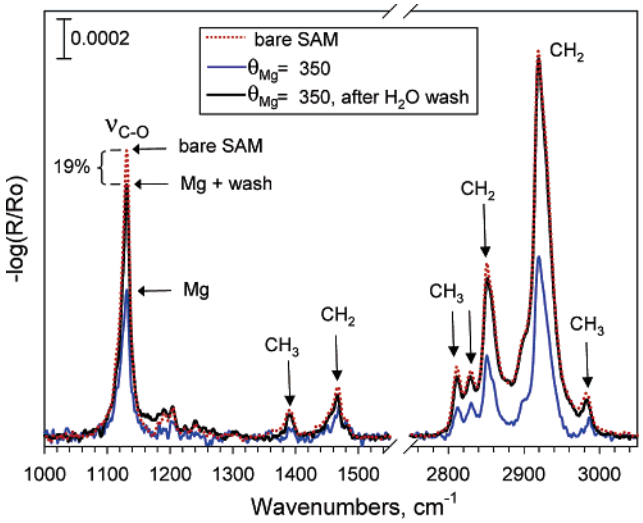

Figure 7. IR spectra of a $-OCH_3$ SAM before Mg dosing (red), after dosing to $\theta_0 = 350$ Mg atoms per SAM molecule (blue), and after water washing of the Mg dosed sample (black). Note that, after rinsing of the Mg-dosed SAM, the spectrum returns almost completely to that of the original SAM, except for very small decreases in the CH_3 modes and a 19% decrease in the ν_{C-O} stretching mode.

is well-organized with the chains primarily in the all-trans conformation.[37]

The spectra show that both the high- and low-frequency regions remain invariant until $\theta_{Mg} \approx 100$. At $\theta_{Mg} > 100$, ν_{C-O} peak intensity starts to attenuate and continues to do so until $\theta_{Mg} = 150$, at which point all modes are observed to attenuate. The initial ν_{C-O} intensity loss can be viewed as the reaction of the deposited Mg and its insertion into either the $O-CH_3$ bond or H_2C-OCH_3 bonds, although the former is more likely because of the closer proximity of this species to the vacuum interface. At $\theta_{Mg} > 150$, all modes attenuate, indicating that a Mg overlayer is forming.

The intensity changes are more easily seen in the IR absorbance difference spectra referenced to the bare SAM (Figure 6). No positive features are observed, indicating that there are no reaction products and that the alkyl changes do not undergo measurable conformation disordering with increasing Mg adsorption. At $\theta_{Mg} = 100$, a small negative feature at 1132 cm^{-1} (ν_{C-O}) indicates that Mg reacts with the $O-CH_3$ bonds, presumably via O−C insertion. At $\theta_{Mg} = 150$, the onset of intensity loss in δ_{CH_3} and the terminal CH_3 C−H stretching modes is observed, along with further ν_{C-O} intensity loss. In addition, small negative peaks are observed for the $-CH_2-$ d^+ and d^- stretches (ν_{CH2}). At $\theta_{Mg} > 200$, the parallel attenuation of all of the IR modes suggests that a Mg overlayer is starting to build up, which causes electromagnetic screening of the IR radiation. The continued presence of the ν_{C-O} stretching mode feature (Figure 4) at the highest total dose, $\theta_{Mg} = 350$, demonstrates that a significant fraction of the C−O bonds have not yet reacted with Mg. From the sticking probability measurements, the coverage of adsorbed Mg at this point is approximately 50 ML (50 Mg atoms/SAM molecule). Thus, this observation suggests that the Mg is nonuniform with bare regions of SAM exposed and/or that a fraction of the adsorbed Mg does not react with a $-OCH_3$ group.

The IRS data also allow us to estimate the sticking probability at the onset of detectable reaction of Mg with the SAM at $\theta_{Mg} \approx 100$. In the limit of all adsorption occurring via chemical reaction with the $-OCH_3$ groups and a detection limit of ~0.01 ML[52] for the stretching mode peak, we estimate that the sticking probability is $(1.5 \pm 0.5) \times 10^{-4}$. This value is considerably smaller than the sticking probability, 5×10^{-2}, measured at $\theta_{Mg} = 100$ using the QCM. There are two likely reasons for the observed discrepancy: (a) a significant fraction of adsorbed Mg atoms at high dose are incorporated in islands and so exert negligible perturbations on the ν_{C-O} mode, and (b) there are sharp, nonlinear changes in the QCM sticking probability at $\theta_{Mg} = 100$ as measured by the QCM. At this point, the sticking probability rises rapidly, indicating the onset of island formation. In agreement with this observation, for $\theta_{Mg} > 100$, we note that the sample surface changes color from the gold of the bare SAM to an increasing black, "sooty" appearance. This suggests that the monolayer is being covered by a nonuniform magnesium overlayer that scatters visible light.

To test the extent of chemical reaction associated with the Mg overlayer, a high dose of magnesium was deposited on the SAM ($\theta_{Mg} = 350$), and then the surface was thoroughly rinsed with deionized water to remove all visible traces of the black overlayer. The IR spectra of the dosed SAM, before and after washing, and of the bare SAM were then compared (Figure 7). There are very small changes in the $-CH_2-$ mode features, essentially within experimental error, between the rinsed sample and the bare SAM, indicating that the alkyl chain organization and packing remain almost unperturbed throughout the Mg deposition and rinsing processes. Because the intensities of these modes return almost to the bare SAM values after rinsing, it is clear that the Mg overlayer has been fully removed and that no molecules are lost via chemical degradation, for example, by penetration of Mg to the Au/S interface. Further, this observation also demonstrates that, for $\theta_{Mg} > 150$, the parallel attenuation of all IR modes arises from physical causes, i.e., electromagnetic screening (Figures 5 and 6).

Second, the intensity of the ν_{C-O} peak decreases by ~18% for the rinsed SAM compared to the bare SAM. This suggests that no more than 18% of the $-OCH_3$ groups on the SAM surface react with the deposited Mg. Note that the small accompanying intensity losses for the CH_3 modes, δ_{CH3}, and the various C−H stretch modes are consistent with this observation. At $\theta_{Mg} = 350$, the estimated surface coverage of Mg is 50 ML, and so the most of the Mg adsorption occurs not via chemical reaction but rather by the formation of islands. Further, the data also suggest that, at $\theta_{Mg} > 150$, most of the adsorbed Mg forms islands at scattered nucleation sites, most likely the reaction centers. The TOF SIMS data support this interpretation because they show that the major pathway for adsorbed Mg is via chemical reaction with $-OCH_3$ groups at low Mg doses ($\theta_{Mg} < 10$), followed by the onset of island formation.

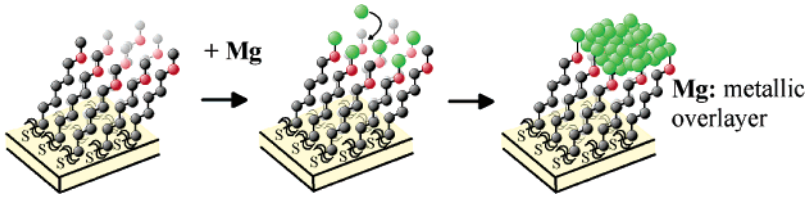

Figure 8. Schematic illustration of the important features of the reaction pathways including complexation and metal overlayer formation. Magnesium is represented in green, oxygen in red, and hydrocarbons in black.

4. Discussion

Both the TOF SIMS and IRS data indicate that deposited Mg reacts with the $-OCH_3$ group to form R−O−Mg species at isolated sites on the surface. Further, the TOF SIMS data show that island formation occurs at very low surface coverages (Mg dose $\theta_{Mg} < 10$). At higher Mg doses, an increasing fraction of adsorbed Mg atoms nucleate into islands, likely by a combination of surface diffusion and direct adsorption onto existing islands. The nucleation centers at low surface coverages are most likely sites at which Mg has reacted with the $-OCH_3$ group.

4.1. Reaction Mechanism. Any proposed model of the magnesium deposition reaction pathway must be able to account for the following observations: (a) the low sticking probability of the deposited magnesium atoms, (b) the reaction of adsorbed Mg with $-OCH_3$ to form R−O−Mg, and (c) the formation of metallic overlayers at high Mg doses. The possible major reaction pathways can be summarized as follows:

Condensation $\quad Mg(g) \leftrightarrow Mg(s) \quad (1)$

Complexation $\quad SAM + Mg(s) \leftrightarrow SAM\cdots Mg \quad (2)$

Bond Insertion $\quad SAM + Mg(s) \rightarrow SAM-Mg \quad (3)$

(Organometallic Formation)

Penetration

$$AuS(CH_2)_{16}OCH_3 + Mg(s) \rightarrow AuMgS(CH_2)_{16}OCH_3 \quad (4)$$

Island Formation $\quad nMg(s) \leftrightarrow [Mg(s)]_n \quad (5)$

where Mg represents the deposited magnesium atoms and SAM denotes the methoxy-terminated SAM adsorbed on the Au surface, $AuS(CH_2)_{16}OCH_3$. The fact that no $MgSH_2^+$, $MgS(CH_2)_x^{\pm}$, and $Au_xMg_yS_z^{\pm}$ ions were observed in the TOF SIMS data indicates that the deposited Mg atoms do not penetrate to the Au/S interface. The IRS data also show no evidence for the disruption of the SAM alkyl chain structure, which would arise if magnesium penetrated through the SAM. Thus, reaction pathway 4 is not operative. From the TOF SIMS data, we also conclude that, upon Mg deposition, a R−O−Mg complex forms (pathway 3). Further, because no $MgOCH_3^+$ ions are observed at the lowest coverages, there is no evidence of a weak reaction solvation between Mg and the terminal group[5−7] (pathway 2). Hence, pathways 1 and 3 are operative. A schematic diagram of the reaction is given in Figure 8.

At low surface doses, magnesium inserts into the $O-CH_3$ bond of the terminal group and the sticking probability is very low, $\sim 5 \times 10^{-3}$. These observations suggest that the adsorption process is a direct activated one; it is only Mg atoms with sufficient energy to overcome the barrier for insertion into the $O-CH_3$ bond that adsorb on the surface. Further, at these low surface doses, $\theta_{Mg} \approx 10$, the TOF SIMS data indicate that clusters or islands are starting to nucleate at the SAM/vacuum interface. However, at $\theta_{Mg} \approx 150$, the IRS data show that very few of the $-OCH_3$ groups have reacted with the deposited Mg. At a dose of $\theta_{Mg} = 350$, no more than 18% of the $-OCH_3$ terminal groups have reacted. Thus, at high doses, the vast majority of the $-OCH_3$ groups remain unreacted. The rapid rise in the sticking coefficient at $\theta_{Mg} \geq 100$ can accordingly be attributed to vapor-deposited Mg becoming trapped on the surface and adsorbing primarily at existing Mg clusters and islands. Thus, there is a switch in the dominant reaction pathways: At low doses, Mg reacts with the $-OCH_3$ groups, and as the Mg deposition continues, the majority of the deposited metal adsorbs on islands/clusters. Given the low percentage of reacted $-OCH_3$ sites, this suggests that the surface reactions might be associated with either specifically oriented $-OCH_3$ groups at the SAM surface or defects, such as domain boundaries.

4.1.1. Formation of Mg−O−R Complex. TOF SIMS and IRS data show evidence for Mg-induced cleavage of the $O-CH_3$ bond at low doses. At these low doses, Mg has a very low sticking probability, $\sim 5 \times 10^{-3}$. In our experiments, Mg is vapor-deposited from an oven source and thus has a wide distribution of incident kinetic energies on the $-OCH_3$-terminated SAM. Assuming that the only fate of a surface-stabilized Mg atom is reaction with the methoxy functional group (i.e., adsorption is a direct activated process), very few Mg atoms striking the surface are able to form a Mg−O−R product. This suggests that only a small fraction of the Mg atoms have sufficient energy to overcome an activation barrier to react with the methoxy group.

We can estimate the energy barrier to the formation of the complex in the following way. In an oven source, metal atoms are generated with a Maxwell distribution of velocities

$$P(v)\,dv = 4\pi\left(\frac{M}{2\pi RT}\right)^{3/2} v^2 \exp\left(\frac{-Mv^2}{2RT}\right) dv$$

where $P(v)\,dv$ is the probability of finding an atom with speed between v and $v + dv$, M is the mass of the atom, R is the gas constant, and T is the temperature of the source. If every deposited, adsorbed magnesium reacts with the terminal $-OCH_3$ group, the probability of reaction is between $\sim 10^{-4}$ (from the IRS data) and 0.005 (from the QCM measurement) and

$$\int_u^{\infty} P(v)\,dv = (1 \times 10^{-4}) - 0.005$$

$$= \int_u^{\infty} 4\pi\left(\frac{M}{2\pi RT}\right)^{3/2} v^2 \exp\left(\frac{-Mv^2}{2RT}\right) dv$$

where u is the speed required for the Mg atom to overcome the reaction barrier, E_a (where $E_a = {}^1/_2 mu^2$). The temperature of the source can be estimated from the Mg vapor pressure, 5×10^{-8} Torr, and is approximately 473 ± 15 K.[53] Using these parameters, we estimate that the minimum energy required to overcome the activation barrier for the formation of the Mg−O−R complex is 38 ± 9 kJ mol^{-1}.

TABLE 1: DFT-Calculated Stabilization Energies for Various Magnesium−Oxygen Complexes

molecule	metal	complex	binding energy (kJ mol^{-1})	metal-O distance (Å)	C-O-C-C dihedral angle	M-O-C angle
Mg $HS(H_2C)_5$ O CH_3	Mg	O···Mg	-4.3	2.69	179.54	
Al $HS(H_2C)_5$ O CH_3	Al	O···Al	-34.0	2.25	155.36	
Mg-O-$(CH_2)_5$-SH	Mg	Mg-O-C	-233	1.79		173.91
Al-O-$(CH)_2$-SH	Al	Al-O-C	-455	1.70		176.77

4.2. Comparison of Magnesium and Aluminum Deposition. Aluminum and magnesium have very similar reactivities; both metals displace hydrogen from steam and tarnish in air. However, their behavior is very different upon deposition on a methoxy-terminated SAM. First, Al has a high initial sticking probability, whereas Mg has a much lower sticking probability. Second, aluminum forms a weak complex with the $-OCH_3$-terminated SAM, Al···OCH_3, and also penetrates to the Au/S interface.[5−7] In contrast, magnesium complexes with the O atom of the methoxy group to form a Mg−O−R structure and does not penetrate to the Au/S interface.

To explore the underlying processes that control the mechanisms of Mg and Al deposition, we carried out density functional calculations for the simple isolated system M + $CH_3O-(CH_2)_5-SH$ and M−O−$(CH)_2$−SH, where M = Mg, Al. The results are summarized in Table 1 and Figure 9.

The calculations show that magnesium forms a very weak complex, Mg···OCH_3, with a binding energy of −4.3 kJ mol^{-1} relative to dissociation to the gas-phase reactants. We note that, at room temperature, kT is ∼2.5 kJ mol^{-1}, and thus, this complex is not very thermally stable. Hence, in agreement with the experimental observations, magnesium does not form a stable Mg···OCH_3 complex and has a low initial sticking probability because it cannot be trapped at the SAM/vacuum interface In contrast, and in agreement with experimental data,[5−7] calculations show that the Al···OCH_3 moiety is stable by −34 kJ mol^{-1}. Thus vapor-deposited Al has a much larger sticking probability on the SAM surface because it can become trapped at the SAM/vacuum interface. Figure 10 displays an illustration of the M···OCH_3 geometry in the SAM molecule. It can be seen that the geometry of the optimized Al···OCH_3 structure is rotated by ∼24.6° from the original $-OCH_3$ terminal group orientation

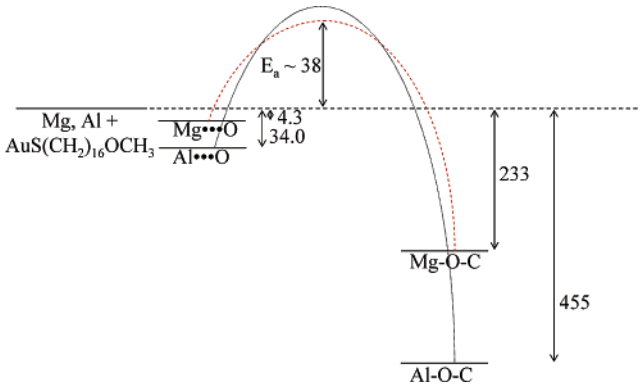

Figure 9. Schematic energy level diagram for the reaction of magnesium and aluminum with the $-OCH_3$-terminated SAM. All energies are given in kJ mol^{-1}. The energy barrier for the Mg reaction is given by the estimate in the text. No value is available for the energy barrier for Al. The diagram is not drawn to scale.

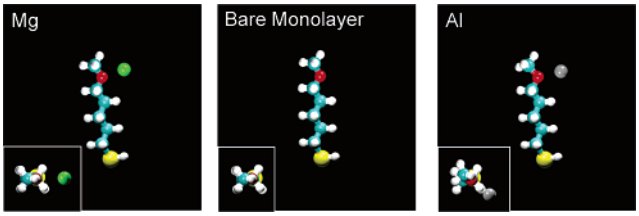

Figure 10. Illustrations of the calculated energy-minimized structures of magnesium and aluminum atoms with the truncated alkanethiolate, $AuS(CH_2)_5OCH_3$. The inset shows the metal atom−molecule interaction as seen from above; the center panel shows the calculated bare SAM structure for reference. The Au atom is shown in yellow, H in white, C in turquoise, O in red, Mg in green, and Al in gray.

(C−O−C−C dihedral angle = 180°). This is not observed with the Mg···OCH_3 interaction and also suggests that the aluminum interaction is much stronger than the magnesium interaction (Table 1).

In agreement with experimental observations, the calculations also show that, for magnesium, insertion into the C−O bond is favorable by −233 kJ mol^{-1}. However, we also note that bond insertion for aluminum is also stable by −455 kJ mol^{-1}. Because we do not observe the formation of Al−O−R complexes experimentally,[5−7] we assume that the reaction barrier is very large.

5. Conclusions

The growth of vapor-deposited magnesium overlayers on a $-OCH_3$-terminated SAM at room temperature initially proceeds by a low-probability bond insertion into the $-OCH_3$ terminal group to form a Mg−OR species, with an estimated activation energy of 38 ± 9 kJ mol^{-1}. These species, in turn, act as nucleation sites for physical adsorption of additional Mg. This leads to an increase in the overall sticking coefficient with increasing Mg coverage and the formation of a nonuniform overlayer. After a dose of θ_{Mg} = 350, analysis indicates that ∼18% of the $-OCH_3$ groups have undergone insertion of Mg into the C−O bond.

These data are in sharp contrast to the cases of Al, Cu, and Ag.[5−7] These metal atoms (M) show high sticking coefficients because of weak solvation interactions with the OCH_3 groups and formation of stable M···OCH_3 complexes. DFT calculations show that the Mg···OCH_3 complex is not stable at room temperature. Thus, in the initial stages, the only adsorption channel is the unlikely formation of the bond-insertion product Mg−O−R, which the calculations show to be stable by −255 kJ mol^{-1}.

In conjunction with previous studies,[1−7,54,55] these experiments provide new insights into the role of dynamic surface processes of metal atoms on organic surfaces. Furthermore, these data will allow more efficient design of metallic contacts for organic and molecular electronic devices, such as PLEDs.

Acknowledgment. The authors acknowledge financial support from the Office of Naval Research, the Air Force Office of Scientific Research, and the National Science Foundation.

References and Notes

(1) Jung, D. R.; Czanderna, A. W. *Crit. Rev. Solid State* **1994**, *19*, 1.
(2) Herdt, G. C.; King, D. E.; Czanderna, A. W. *Z. Phys. Chem.* **1997**, *202*, 163.
(3) Hooper, A.; Fisher, G. L.; Konstadinidis, K.; Jung, D.; Nguyen, H.; Opila, R.; Collins, R. W.; Winograd, N.; Allara, D. L. *J. Am. Chem. Soc.* **1999**, *121*, 8052.
(4) Fisher, G. L.; Hooper, A. E.; Opila, R. L.; Allara, D. L.; Winograd, N. *J. Phys. Chem. B* **2000**, *104*, 3267.

(5) Fisher, G. L.; Walker, A. V.; Hooper, A. E.; Tighe, T. B.; Bahnck, K. B.; Skriba, H. T.; Reinard, M. D.; Haynie, B. C.; Opila, R. L.; Winograd, N.; Allara, D. L. *J. Am. Chem. Soc.* **2002**, *124*, 5528.

(6) Walker, A. V.; Tighe, T. B.; Reinard, M. D.; Haynie, B. C.; Allara, D. L.; Winograd, N. *Chem. Phys. Lett.* **2003**, *369*, 615.

(7) Walker, A. V.; Tighe, T. B.; Cabarcos, O.; Reinard, M. D.; Haynie, B. C.; Uppili, S.; Allara, D. L.; Winograd, N. *J. Am. Chem. Soc.* **2004**, *126*, 3954.

(8) Chen, J.; Reed, M. A.; Rawlett, A. M.; Tour, J. M. *Science* **1999**, *286*, 1550.

(9) Metzger, R. M.; Xu, T.; Peterson, I. M. *J. Phys. Chem. B* **2001**, *105*, 7280.

(10) Chen, Y.; Ohlberg, D. A. A.; Li, X.; Stewart, D. R.; Williams, R. S.; Jeppesen, J. O.; Nielsen, K. A.; Stoddart, J. F.; Olynick, D. L.; Anderson, E. *Appl. Phys. Lett.* **2003**, *82*, 1610.

(11) Shuler, S. F.; Davis, G. M.; Morris, J. R. *J. Chem. Phys.* **2002**, *116*, 9147.

(12) Day, B. S.; Shuler, S. F.; Ducre, A.; Morris, J. R. *J. Chem. Phys.* **2003**, *119*, 8064.

(13) Ferguson, M. K.; Lohr, J. R.; Day, B. S.; Morris, J. R. *Phys. Rev. Lett.* **2004**, *92*, 073201.

(14) Day, B. S.; Morris, J. R. *J. Chem. Phys.* **2005**, *122*, 234714.

(15) Lohr, J. R.; Day, B. S.; Morris, J. R. *J. Phys. Chem. B* **2005**, *109*, 15469.

(16) Lohr, J. R.; Day, B. S.; Morris, J. R. *J. Phys. Chem. A* **2006**, *110*, 1645.

(17) Rettner, C. T.; Auerbach, D. J.; Tully, J. C.; Kleyn, A. W. *J. Phys. Chem.* **1996**, *100*, 13023.

(18) Tully, J. C. *Annu. Rev. Phys. Chem* **2000**, *51*, 153.

(19) Somorjai, G. A. *Introduction to Surface Chemistry and Catalysis*; John Wiley & Sons: New York, 1994.

(20) King, D. A.; Wells, M. G. *Surf. Sci.* **1972**, *29*, 245.

(21) Zaporojtchenko, V.; Behnke, K.; Thran, A.; Strunksus, T.; Faupel, F. *Appl. Surf. Sci.* **1999**, *144*−*145*, 355.

(22) Thran, A.; Kiene, M.; Zaporojtchenko, V.; Faupel, F. *Phys. Rev. Lett.* **1999**, *82*, 1903.

(23) Zaporojtchenko, V.; Behnke, K.; Strunksus, T.; Faupel, F. *Surf. Sci.* **2000**, *454*−*456*, 412.

(24) Zaporojtchenko, V.; Behnke, K.; Strunksus, T.; Faupel, F. *Surf. Interface Anal.* **2000**, *30*, 439.

(25) Ma, Z. H.; Lim, S. L.; Tan, K. L.; Li, S.; Kang, E. T. *Surf. Sci.* **2000**, *454*−*456*, 995.

(26) Ma, Z. H.; Lim, S. L.; Tan, K. L.; Li, S.; Kang, E. T. *J. Mater. Sci.*−*Mater. El.* **2000**, *11*, 311.

(27) Wong, P. C.; Li, Y. S.; Mitchell, K. A. R. *Appl. Surf. Sci.* **1995**, *84*, 245.

(28) Kono, M.; Wong, P. C.; Li, Y. S.; Mitchell, K. A. R. *Surf. Rev. Lett.* **2000**, *7*, 227.

(29) Lim, V. W. L.; Kang, E. T.; Neoh, K. G.; Huang, W. *J. Vac. Sci. Technol. A* **2001**, *19*, 2680.

(30) Bröms, P.; Birgerson, J.; Salaneck, W. R. *Synth. Met.* **1997**, *88*, 255.

(31) Li, S.; Kang, E. T.; Ma, Z. H.; Tan, K. L. *Surf. Interface Anal.* **2000**, *29*, 95.

(32) Susac, D.; Kono, M.; Wong, K. C.; Mitchell, K. A. R. *Appl. Surf. Sci.* **2001**, *174*, 43.

(33) Nowak, S.; Mauron, R.; Dietler, G.; Schlapbach, L. XPS Study of Metal−Polymer Interfaces after Polymer Surface Treatment by Ion and Plasma Techniques. In *Metallized Plastics 2*; Mittal, K. L., Ed.; Plenum Press: New York, 1991; p 233.

(34) Nowak, R. W.; Collaud, M.; Dietler, G.; Gröning, P.; Schlapbach, L. *J. Vac. Sci. Technol. A* **1993**, *11*, 481.

(35) Collaud, M.; Nowak, S.; Küttel, O. M.; Schlapbach, L. *J. Adhes. Sci. Technol.* **1994**, *8*, 435.

(36) Collaud, M.; Groening, P.; Nowak, S.; Schlapbach, L. *J. Adhes. Sci. Technol.* **1994**, *8*, 1115.

(37) Nuzzo, R. G.; Dubois, L. H.; Allara, D. L. *J. Am. Chem. Soc.* **1990**, *112*, 558.

(38) Bain, C. D.; Evall, J.; Whitesides, G. M. *J. Am. Chem. Soc.* **1989**, *111*, 7155.

(39) Laibinis, P. E.; Bain, C. D.; Nuzzo, R. G.; Whitesides, G. M. *J. Phys. Chem.* **1995**, *99*, 7663.

(40) Dubois, L. H.; Nuzzo, R. *Annu. Rev. Phys. Chem* **1992**, *43*, 437.

(41) Laibinis, P. E.; Whitesides, G. M.; Allara, D. L.; Tao, Y.-T.; Parikh, A. N.; Nuzzo, R. G. *J. Am. Chem. Soc.* **1991**, *113*, 7152.

(42) Schreiber, F. *Prog. Surf. Sci.* **2000**, *65*, 151.

(43) Braun, R. M.; Blenkinsopp, P.; Mullock, S. J.; Corlett, C.; Willey, K. F.; Vickerman, J. C.; Winograd, N. *Rapid Commun. Mass Spectrom.* **1998**, *12*, 1246.

(44) Beamson, G.; Briggs, D.; Davies, S. F.; Fletcher, I. W.; Clark, D. T.; Howard, J.; Gelius, U.; Wannberg, B.; Balzer, P. *Surf. Interface Anal.* **1990**, *15*, 541.

(45) Gelius, U.; Wannberg, B.; Baltzer, P.; Fellnerfeldegg, H.; Carlsson, G.; Johansson, C. G.; Larsson, J.; Munger, P.; Vegerfors, G. *J. Electron Spectrosc. Relat. Phenom.* **1990**, *52*, 747.

(46) Sauerbray, G. *Z. Phys.* **1959**, *155*, 206.

(47) Dixon, M. C. Application of the Quartz Crystal Microbalance to Self-Assembled Monolayers. M.S. Thesis, The Pennsylvania State University, University Park, PA, 2002.

(48) Frisch, M. J.; Trucks, G. W.; Schlegel, H. B.; Scuseria, G. E.; Robb, M. A.; Cheeseman, J. R.; Zakrzewski, V. G.; Montgomery, J. A., Jr.; Stratmann, R. E.; Burant, J. C.; Dapprich, S.; Millam, J. M.; Daniels, A. D.; Kudin, K. N. O.; Strain, F. M. C.; Farkas, O.; Tomasi, J.; Barone, V.; Cossi, M.; Cammi, R.; Mennucci, B.; Pomelli, C.; Adamo, C.; Clifford, S.; Ochterski, J.; Petersson, G. A.; Ayala, P. Y.; Cui, Q.; Morokuma, K.; Malick, D. K.; Rabuck, A. D.; Raghavachari, K.; Foresman, J. B.; Cioslowski, J.; Ortiz, J. V.; Baboul, A. G.; Stefanov, B. B.; Liu, G.; Liashenko, A.; Piskorz, P.; Komaromi, I.; Gomperts, R.; Martin, R. L.; Fox, D. J.; Keith, T.; Al-Laham, M. A.; Peng, C. Y.; Nanayakkara, A.; Challacombe, M.; Gill, P. M. W.; Johnson, B.; Chen, W.; Wong, M. W.; Andres, J. L.; Gonzalez, C.; Head-Gordon, M.; Replogle, E. S.; Pople, J. A. *Gaussian 98*, revision A.9; Gaussian Inc.: Pittsburgh, PA, 1998

(49) The signal-to-noise ratio of the experiments was ±0.2 Hz, and a Mg coverage of 1 ML (1 Mg atom/SAM molecule) is 1.5 Hz. In general, it is very difficult/impossible to detect a signal when the signal-to-noise ratio is less than 2 or 3. (Skoog, D. A.; Holler, F. J.; Nieman, T. A. *Principles of Instrumental Analysis*, 5th ed.; Brooks/Cole Thomson Learning: Philadelphia, PA, 1998] Thus, the first surface Mg coverage that could be measured is 0.4 ML. The fluctuations in the QCM signal are due to instrument noise, slight temperature changes, fluctuations in the Mg flux, and inherent fluctuations in the partitioning between Mg adsorption and scattering.

(50) Ong, T. H.; Davies, P. B.; Bain, C. D. *Langmuir* **1993**, *9*, 1836.

(51) Allan, A.; McKean, D. C.; Perchard, J.-P.; Josien, M.-L. *Spectrochim. Acta* **1971**, *27A*, 1409.

(52) The detection limit is determined by factors such as the infrared adsorption cross section. We estimated the detection limit for the CO stretch (1132 cm^{-1}) as ∼0.01 ML based on the observed rms signal-to-noise ratio of $\sim 3 \times 10^{-5}$ and a peak height of the CO stretch for a full monolayer of $\sim 3 \times 10^{-3}$.

(53) *Vapor Pressure for Selected Elements*; Veeco Instruments Inc.: Woodbury, NY, 2006; available at http://www.topometrix.com/learning/learning_vaporelements.asp (accessed Sep 15, 2006).

(54) Walker, A. V.; Tighe, T. B.; Haynie, B. C.; Uppili, S.; Allara, D. L.; Winograd, N. *J. Phys. Chem. B* **2005**, *109*, 11263.

(55) Walker, A. V.; Tighe, T. B.; Stapleton, J. J.; Haynie, B. C.; Allara, D. L.; Winograd, N. *Appl. Phys. Lett.* **2004**, *84*, 4008